http://dx.doi.org/10.5012/bkcs.2011.32.10.3821

Application of Interpolation Method to Magnetic Resonance Imaging for Removal of Radio-Frequency Noise

Junghun Cho,[†] Sangdoo Ahn,[‡] Chang-Hyun Oh,[§] Janggun Cho,[†,‡] Eun Kyoung Ryu,[†] Jee-Hyun Cho,[†,‡,*] and Chulhyun Lee[†,*]

[†]*Division of Magnetic Resonance Research, Korea Basic Science Institute, Ochang, Cheongwon, Chungbuk 363-883, Korea*
[*]*E-mail: jhcho@kbsi.re.kr, chulhyun@kbsi.re.kr*
[‡]*Department of Chemistry, Chung-Ang University, Seoul 156-756, Korea*
[§]*Dept. of Electronics and Information Engineering, Korea University, Jochiwon, Yeongi, Chungnam 339-700, Korea*
Received June 3, 2011, Accepted August 18, 2011

Key Words : Image processing, RF noise, Interpolation method, De-noising method

In magnetic resonance imaging (MRI), noise filtering is widely used to improve image quality,[1-3] which is necessitated by many applications. For example, noise filtering is very important as a pre-processing tool in image segmentation,[4,5] which is useful for the detection of many diseases including brain tumors.[6-8] Therefore, many studies have been conducted with an aim of reducing noise or artifacts, such as radio-frequency (RF) noise[9,10] or motion,[11,12] chemical shift,[13,14] eddy current,[15,16] and truncation artifacts[17] in MR images.

In this study, we focus on RF noise removal. RF noise usually has a stripe-like shape and is caused by unwanted external RF signals.[18] There exist a few methods to reduce this noise, such as using an RF shield,[19] adjusting spectral bandwidth, and changing readout direction. However, RF shields are expensive and changing the receiver bandwidth or the readout direction does not completely remove noise; instead, it simply moves the noise away from the region of interest.

Post-processing methods can be used as an alternative approach for RF noise removal. We first considered the possibility of separating the noise by handling pixel values in the frequency domain. However, even though it is assumed that this method can determine the specific frequency corresponding to the external RF noise region, a part of the signal at that frequency may originate from the sample. Therefore, we cannot completely remove the signal at the detected specific frequency. We also considered image segmentation in the image domain as alternative method for noise removal. However, in a given region, RF noise is distributed randomly, and therefore, this method is not effective. Thus, we eliminated two types of post-processing methods, i.e., image segmentation and any frequency-domain-based method.

Next, we applied three well-known de-noising methods as alternative post-processing methods for RF noise removal. The adaptive median filter, which takes the median value of the gray level of surrounding pixels as the value of each pixel, is used to reduce the scattered dot noise.[20] The Wiener filter and the Lucy Richardson (LR) method use their respective algorithms to generate a clear image from a given noisy and blurred image.[21]

In this article, we examined the effectiveness of these three de-noising methods (Adaptive Median Filter, Wiener Filter, and Lucy Richardson Method). Finally, we propose the use of the Interpolation Method as a new de-noising method, which, as we found, is more intuitive and effective for RF noise removal than the conventional methods.

First, we searched for the RF noise range in the image domain. Because the RF noise in the samples used for this study is distributed across all rows in certain columns, as shown in Figure 1(a), we found the specific columns in which the pixel values are larger than the threshold pixel value for the background region. We set the threshold pixel value as 50 at the 256 gray level scale, because the maximum background pixel value is usually less than 10. Then, we applied the four aforementioned post-processing methods to the selected RF noise range. The results of this experiment are as follows.

Adaptive Median Filter. The noise has a stripe-like shape, which is highlighted by an arrow in Figure 1(a). This indicates that this noise is a type of RF noise. Considering that the noise is spread in the white-stripe region, we applied the adaptive median filter, a simple conventional method, to erase small, dispersed noise. Unlike the standard median filter, the adaptive median filter uses a two-level algorithm to reduce blur while preserving detailed structures.[20] However, the adaptive median filter could not eliminate the

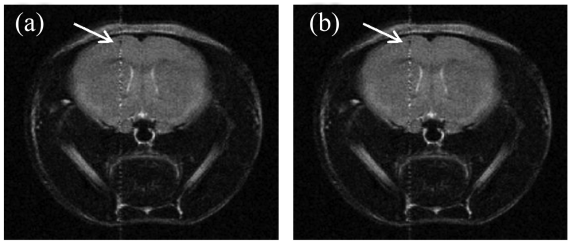

Figure 1. (a) Original MR image and (b) Image modified by using adaptive median filter. The noise-containing region is indicated by an arrow.

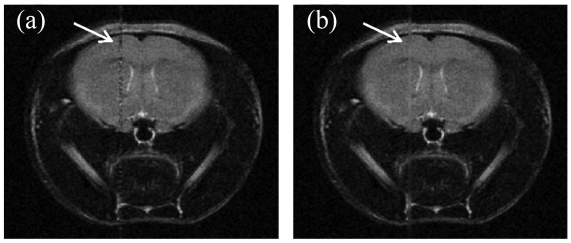

Figure 2. Images modified using two different types of Wiener filter: (a) Wiener filter and (b) constrained deconvolution method.

white-stripe noise, as can be seen in Figure 1(b). This implies that the median value of the pixels surrounding the white-stripe noise contains the noise signal because the noise is distributed densely in the white-stripe region.

Wiener Filter. The Wiener filter, one of the most popular linear image-restoration methods, was used to de-noise the white-stripe region. As shown in Eq. (1), this method is used to find the best estimate of f (de-noised image) based on the given g (noisy image) with specific constraints. H is a point spread function (PSF) and n is an additive noise component. Because we considered only noise, we assumed $H = 1$.

$$g = Hf + n \tag{1}$$

The constraints are as follows. (a) If we seek an estimate of f, which minimizes the cost function $Q = n^T n = |Hf - g|^2$, it is considered as the Wiener filter. (b) If the cost function $Q = |Lf|^2 - \lambda\{|Hf|^2 - |n|^2\}$, it is considered as the constrained deconvolution method, where L and λ are the Laplacian operator and the Lagrange multiplier, respectively.[21]

As can be seen in Figure 2(a), the noise was not removed by the Wiener filter. The intensity of the stripe region changed from white to black. This implies that the Wiener filter simply changed the gray level of the noise pixels to zero. This is because the occurrences of noise are so densely packed in the stripe region that they cannot be considered as noise by the Wiener filter. Figure 2(b) shows that the noise was smoothed by the constrained deconvolution method. This was attributed to the balance between the Laplacian operator effect and the condition that minimizes noise. However, traces of white-stripe noise still exist. When used as a Wiener filter, the constrained deconvolution method is also unable to recognize white-stripe region as noise because of the very high noise density in the region.

Lucy Richardson (LR) Method. The LR method includes an iterative algorithm that attempts to determine the best estimate of f with the constraint that noise should be minimized [Eq. (2)].

$$f_{k+1} = f_k + [g - Hf_k] \tag{2}$$

Figure 3 shows that the LR method had almost no effect on the white-stripe noise compared with the original image (Fig. 1(a)). The LR method is based on the premise that noise in the output is governed by the Poisson distribution;[21] therefore, it can be used when the probability of the occurrence of noise is low. In our case, the noise in the white-stripe region was high. Therefore, this algorithm was not effective.

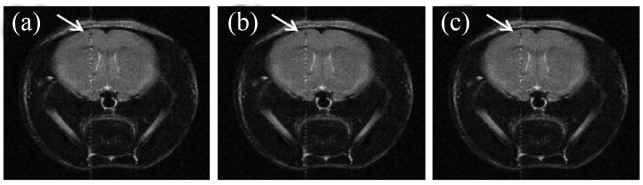

Figure 3. Images modified using LR method: (a) 20, (b) 50, and (c) 100 iterations.

Interpolation Method. Because the width of the noise is narrow (3-5 pixels), a new de-noising concept, i.e., the interpolation method, was applied. Because the noise has a stripe-like shape, only two neighboring pixels near the noise region in the same row were used for interpolation, instead of the usual four pixels used for bilinear interpolation. There are two interpolation methods (x and y indicate row and column, respectively.):

Method 1. Fix two endpoints (y_{min}, y_{max}) and vary the interpolation ratio (α_i).

$$I_{method1}(x, y_i) = I(x, y_{min})\alpha_i + I(x, y_{max})(1-\alpha_i) \tag{3}$$

Method 2. Vary two endpoints (y_{i-}, y_{i+}) and fix the interpolation ratio (β).

$$I_{method2}(x, y_i) = I(x, y_{i-})\beta + I(x, y_{i+})(1-\beta) \tag{4}$$

where $\alpha_i = \mu_i/\Delta y$, $\mu_i = y_i - min(y_i)$, $y_{i-} = y_i - \Delta y$, $y_{i+} = y_i + \Delta y$, $\beta = \Delta y/2$, I is pixel value, and Δy is the width of the white-stripe noise ($y_{max} - y_{min}$). The values of y_{min}, y_{max}, α, and β can be adjusted to effectively obtain the desired result. As shown in Figure 4, the white-stripe noise was clearly erased by both the interpolation methods and there was almost no distortion.

In summary, we discussed various image processing methods to remove the white-stripe noise that originates from external RF noise. We confirmed that the conventional image processing methods have some limitations in the removal of white-stripe noise. Also, we proposed the application of the interpolation method for de-noising, which proved to be simpler and more powerful for RF noise removal than the conventional de-noising methods. This method can be used for the removal of many noise types except in the case that one particular pixel contains a considerable amount of information. Furthermore, this study opens up the possibility of developing interpolation methods for canceling specific noises, which is expected to be useful for efficient disease detection.

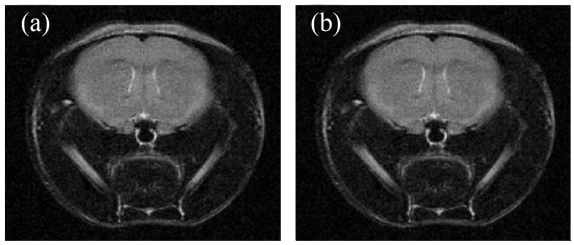

Figure 4. Images modified using proposed interpolation methods: (a) Method 1 and (b) Method 2.

Experimental Section

Animals and Magnetic Resonance Imaging. The animal experiments were carried out according to a protocol approved by the KBSI committee (KBSI-AEC1107). Nine-week-old Balb/C (male) mice (Japan SLC, Inc; 25 g body weight) were used for brain imaging. All MRI experiments were performed at KBSI in Ochang, Korea, using a 4.7 T animal MRI scanner (BioSpec 47/40; Bruker, Germany) equipped with a 25-mm volume coil. The experimental data were obtained and analyzed using ParaVision 4.0 (Bruker, Germany). The mice were anesthetized using 1.5-2% isoflurane in a mixture of N_2O/O_2 = 7/3 for the duration of the MRI. T_2 images were acquired using the rapid acquisition with refocused echo (RARE) pulse sequence. The imaging parameters were as follows: echo time (TE) = 90.0 ms, repetition time (TR) = 5 s, field of view (FOV) = 2.0 × 2.0 cm^2, slice thickness = 1 mm, matrix size = 256 × 256, and spectral bandwidth = 50 kHz.

Image Processing. All conventional image processing methods used the built-in functions in Matlab Image Toolbox (MathWorks, Natick, MA, USA). The codes used for interpolation were written in Matlab. To improve the effectiveness of the interpolation method, we applied it to a range wider than the detected noise range. More specifically, we set Δy as $y_{max} - y_{min} + 8$ and $min(y_i)$ as $min(y_i) - 2$ in interpolation method 1, and we set Δy as $y_{max} - y_{min} + 5$ in interpolation method 2.

Acknowledgments. This research was supported by Korea Basic Science Institute grant (T31404), NAP of the Korean Research Council of Fundamental Science & Technology (PGB042) and the Korea Research Foundation Grant funded by the Korean Government (MOEHRD, Basic Research Promotion Fund) (KRF-2007-331-C00137).

References

1. Khademi, A.; Venetsanopoulos, A.; Moody, A. R. *IEEE Signal Processing Letters* **2010**, *17*, 989.
2. Liu, H.; Pan, N.; Song, E.; Green, R. *Magn. Reson. Imaging* **2010**, *28*, 1485.
3. Ardizzone, E.; Pirrone, R.; Gallea, R.; Gambino, O. *Computer-Based Medical Systems*; 2008. CBMS '08. 21st IEEE International Symposium on 2008; p 29.
4. Clarke, L. P.; Velthuizen, R. P.; Camacho, M. A.; Heine, J. J.; Vaidyanathan, M.; Hall, L. O.; Thatcher, R. W.; Sibiger, M. L. *Magn. Reson. Imaging* **1995**, *13*, 343.
5. Dakua, S. P.; Sahambi, J. S. *India Conference (INDICON), 2009 Annual IEEE* Gujarat 2009; p 1.
6. Harati, V.; Khayati, R.; Farzan, A. *Computers in Biology and Medicine* **2011**, *41*, 483.
7. Nie, J.; Xue, Z.; Liu, T.; Young, G. S.; Setayeshi, K.; Guo, L.; Wong, S. T. C. *Computerized Medical Imaging and Graphics* **2009**, *33*, 431.
8. Dou, W.; Ruan, S.; Chen, Y.; Bloyet, D.; Constans, J. M. *Image. Vision. Comput.* **2007**, *25*, 164.
9. Negishi, M.; Pinus, A. B.; Constable, R. T. *IEEE T. Bio-Med. Eng.* **2007**, *54*, 1725.
10. Oshiro, T.; Sinha, U.; Lu, D.; Sinha, S. *J. Comput. Assist. Tomo.* **2002**, *26*, 308.
11. Zoroofi, R. A.; Sato, Y.; Tamura, S.; Naito, H. *IEEE Transactions on Medical Imaging* **1996**, *15*, 768
12. Nguyen, T. D.; Ding, G.; Watts, R.; Wang, Y. *Magn. Reson. Imaging* **2001**, *19*, 951.
13. Cheng, Y. C.; Chen, J. H.; Wang, T. T.; Lin, T. T. *Magn. Reson. Imaging* **2009**, *27*, 1429.
14. Maeda, A.; Yokoyama, T. *IEEE T. Med. Imaging* **1989**, *8*, 8.
15. Jezzard, P.; Barnett, A. S.; Pierpaoli, C. *Magn. Reson. Med.* **1998**, *39*, 801.
16. Ahn, C. B.; Cho, Z. H. *IEEE T. Med. Imaging* **1991**, *10*, 47.
17. Sarkar, S.; Herlein, K.; Hu, X. *Magn. Reson. Imaging* **2002**, *20*, 743.
18. Hashemi, R. H.; Bradley, W. G.; Lisanti, C. J. *MRI The Basics Second Edition*; Lippincott Wialliams & Wilkins, 2004; pp 187-218.
19. Jin, J.; Magin, R. L.; Shen, G.; Perkins, T. *IEEE T. Bio-Med. Eng.* **1995**, *42*, 840.
20. Gonzalez, R. C.; Woods, R. E.; Eddins, S. L. *Digital Image Processing USING MATLAB*, Prentice Hall, 2004; pp 149-204.
21. Solomon, C.; Breckon, T. *Fundamentals of Digital Image Processing A Practical Approach with Examples in Matlab*; Wiley-Blackwell: 2011; pp 147-167.